Catalyst deactivation by coke formation in microporous and desilicated zeolite H-ZSM-5 during the conversion of methanol to hydrocarbons

Catalyst deactivation by coke formation in microporous and desilicated zeolite H-ZSM-5 during the conversion of methanol to hydrocarbons

Francesca Lønstad Bleken[1], Katia Barbera[2], Francesca Bonino[3], Unni Olsbye[1], Karl Petter Lillerud[1], Silvia Bordiga[3,*], Pablo Beato[4,*] Ton V. W. Janssens[4], Stian Svelle[1,*]

[1] inGAP Center of Research Based Innovation/Center for Materials Science and Nanotechnology (SMN), University of Oslo, Department of Chemistry, N-0315 Oslo, Norway

[2] Department of Industrial Chemistry and Materials Engineering, University of Messina V.le F. Stagno d'Alcontres 31, I-98166, Messina, Italy

[3] Department of Chemistry, NIS Centre of Excellence, and INSTM Centro di Riferimento University of Turin, Via Quarello 15, I-10135, Turin, Italy

[4] Haldor Topsøe, Nymøllevej 55, DK-2800 Kgs. Lyngby, Denmark

KEYWORDS: Hierarchical; MTG; MTO; MTH; desilication; mesoporous; characterization

Abstract: Desilication has become a standard method to prepare mesoporous zeolite catalysts that display improved lifetime or resistance towards deactivation in hydrocarbon transformation processes involving coking. In this contribution, the deactivation behaviors of a regular, commercial ZSM-5 catalyst and its mesoporous, desilicated counterpart have been investigated and compared. After partial deactivation in the conversion of methanol to hydrocarbons at elevated reaction pressure, the catalyst beds were fractionated from top to bottom of the reactor. These fractions were analyzed by several spectroscopic techniques, gas adsorption measurements, thermogravimetry, coke analysis by a catalyst dissolution/extraction protocol, and measurements of residual activity for the individual catalyst fractions. Remarkable differences between the desilicated and the parent H-ZSM-5 catalysts are seen, in particular with respect to the mode of deactivation along the catalyst beds. It appears that the more uniform deactivation of the desilicated catalyst is due to a complex interplay among alterations of porosity, activity, and rate of deactivation upon desilication.

1. Introduction

Zeolites are widely employed as catalysts in the petrochemical and refinery industries [1]. These materials may contain Brønsted acid active sites dispersed within a microporous network, leading to shape selective catalysis. The size, shape, and dimensionality of the zeolite catalyst pores determine the catalytic performance, with respect to both product selectivity and catalyst deactivation behavior [2,3,4,5,6]. In most zeolite catalyzed hydrocarbon transformation reactions, loss of catalyst activity due to coke deposition occurs. This may be remedied by oxidative catalyst regeneration. However, such treatments often lead to a gradual loss of crystallinity caused by steam exposure at the elevated temperatures required for regeneration [7,8,9]. This imposes limits on the overall catalyst lifetime in an industrial application. The incentives for attempts to reduce coking or to reduce its effects are therefore significant. To limit the actual deposition of coke beyond what may be achieved by optimizing the reaction conditions would require a fundamental understanding of catalyst structure-deactivation relationships. This is a formidable task for processes where hydrocarbons are converted; however, to limit the effects of coke deposition might be more manageable. One particularly promising approach is to synthesize mesoporous or hierarchical zeolite catalysts [10,11,12,13]. This may be achieved by a variety of methods such as hard templating, the use of surfactants, or various post synthesis treatments [14,15,16,17,18]. Among these methods, mesopore generation by post synthesis treatments with dilute alkaline solutions, known as desilication, is particularly appealing, primarily due to the simplicity and reasonably broad applicability of this approach, as recently reviewed by Verboekend and Perez-Ramirez [19]. Substantial improvements in deactivation resistance have been reported for such desilicated zeolite catalysts [10,11]. However, the underlying reasons for the improved deactivation resistance have not been described satisfactorily. This is a complex issue, and it has been proposed that mesoporosity might lead to enhanced mass transfer of

coke precursors [11,13], or possibly an increased tolerance for coke deposition i.e. that a higher coke loading is required to deactivate the catalyst [12]. An alternative or contributing cause could be related to changes in acidic properties and/or the rearrangement of internal defects during desilication, as such defects are known to be detrimental for the catalytic performance [10,20,21].

In this report we characterize and compare two partially deactivated H-ZSM-5 zeolite catalysts, one desilicated and the other purely microporous. These catalysts were employed in the conversion of methanol to hydrocarbons (MTH). This reaction may be considered to constitute a final step in the upgrading of natural gas, coal, or biomass into liquid fuels or light alkenes for petrochemical production [2]. Notably, the catalytic reactions have been performed in fixed bed reactors at industrially relevant reaction pressures, i.e. not typical laboratory conditions. This work is also unusual in that we have separated the catalyst beds into fractions after partial deactivation and submitted each fraction to several different characterization and analysis methods. This allowed us to investigate if and how the desilication affects the deactivation behavior at different points in the bed. Of particular relevance to this aspect of our study is a recent report by Schultz [22], where the catalyst activity and deactivation of several non-mesoporous zeolites have been investigated axially along the fixed bed reactor. We have employed several spectroscopic techniques, gas adsorption measurements, thermogravimetry, coke analysis by a catalyst dissolution/extraction protocol, and measurements of residual activity for these catalyst fractions in order to study the deactivation phenomena.

2. Experimental

2.1. Catalysts and desilication procedure

In this study, two H-ZSM-5 catalyst samples will be compared: A commercial catalyst (supplied by Zeochem International and designated PZ-2/100H; stated Si/Al ratio 50) and its desilicated, mesoporous counterpart. These catalysts will be referred to as ZSM-5 and D-ZSM-5 respectively. The mesoporous catalyst (D-ZSM-5) was prepared by desilication according to the following procedure. The unmodified ZSM-5 starting material was treated with a 0.3 M NaOH solution (33 mL solution per gram catalyst material) for 30 minutes at 343 K, followed by cooling in an ice-bath to stop the desilication, and then washing with water and centrifuging three times. The acidic form of the desilicated zeolite was produced by two consecutive ion exchanges with a buffer solution of 1.7 M NH_4NO_3/0.94 M NH_3, using 10 mL solution per gram catalyst, at 353 K under stirring for two hours. After each exchange, the NH_4-forms of the zeolites were filtered, washed with water, and dried in air at 383 K. The final H-form of the D-ZSM-5 zeolite was obtained by heating the NH_4-form in air to 823 K for 3 hours.

2.2. Characterization of fresh catalysts

The fresh catalysts (ZSM-5 and D-ZSM-5) were characterized using FT-IR with CO and pyridine as probes, NH_3-TPD, SEM, elemental analysis, nitrogen adsorption, and X-ray diffraction. Experimental details are given in the supplementary material.

2.3. Catalytic testing

Two experimental fixed bed set-ups were used for the catalytic testing, one at high pressure (the initial catalytic test to build up coke in the catalysts) and one at atmospheric

pressure (as a characterization tool after deactivation at high pressure, see below). A regular top to bottom flow pattern was employed.

In the high-pressure experiments, a stainless steel tube reactor was filled with 3 or 6 g of the zeolite in a 0.3-0.6 mm sieve fraction. The reaction was carried out at 350 °C and 15 barg, using a feed of 14 or 28 % methanol in N_2 flow of 100 Nml/min (giving a WHSV of 0.75 $gg^{-1}h^{-1}$) and stopped after 160 h on stream. Methanol breakthrough was not observed after this reaction time and methanol conversion was thus still 100 %.

The catalyst bed diameter was the same for both catalysts (internal reactor diameter 6 mm). However, due to a significant difference in density (the desilicated catalyst has a much lower density), different catalyst amounts had to be used in order to maintain the same bed height (200 mm). As a consequence, to keep the WHSV constant, different partial pressures of methanol were employed. It cannot be ruled out that this difference in experimental set-up might influence the catalyst performance and deactivation behavior. Thus, in the following, we will limit the discussion to cover only the major features observed.

After 160 h on stream, the catalyst beds were divided into either 10 or 5 parts, corresponding to different axial positions in the reactor. The individual bed fractions were then characterized by different methods. The details of the high pressure catalytic testing are summarized in Table 1.

Table 1. Experimental conditions of high pressure conversion of methanol to hydrocarbons.

Catalyst	WHSV ($gg^{-1}h^{-1}$)	Catalyst mass	Methanol concentration	Total pressure	Number of fractions
ZSM-5	0.75	6 g	28 %	15 barg	10
D-ZSM-5	0.75	3 g	14 %	15 barg	5

In order to monitor the residual catalytic activity of each catalyst fraction, further catalytic tests were carried out at atmospheric pressure. These low pressure experiments were carried out for a selection of the individual fractions at 350 °C. 130 mbar methanol in a He stream was reacted over 20 mg catalyst placed in a fixed bed micro reactor, resulting in a WHSV of 5 $gg^{-1}h^{-1}$. Note that this feed rate is substantially higher than in the high pressure tests. These experiments were left on stream over night and no deactivation could be observed during reaction, except minor deviations for the first analysis point, The products were analyzed with an online Agilent 6890 A GC-FID equipped with a Supelco SPB-5 capillary column (60 m, 0.530 mm i.d., stationary phase thickness 3μm).

2.4. Analysis of partially deactivated catalysts

Powdered samples of partially deactivated catalyst obtained from the individual zeolite fractions taken from the reactor after 160 h of methanol conversion in the high pressure catalytic reactor (Table 1) were characterized by several methods to examine the mode of deactivation. For the spectroscopic characterization, samples were exposed to laboratory air and thus rehydrated prior to the measurements.

Diffuse Reflectance UV/Vis spectra (DRUV/Vis) were recorded with a Cary 5000 spectrophotometer in order to characterize the nature of the entrapped species.

Parallel studies were performed also by Diffuse Reflectance Infrared Fourier Transform Spectroscopy (DRIFTS) by using the SMART collector set-up implemented in a Nicolet spectrophotometer. Spectra have been collected on powder samples diluted in KBr at 4 cm^{-1} resolution in air.

BET surface areas were determined by N_2 adsorption at -196 °C on an ASAP2020 Micromeritics instrument. Prior the measurements, the samples were outgassed at 150 °C

overnight to release water. Different types of porosities were evaluated through the t-plot method (Harkins and Jura universal thickness curve).

Retained hydrocarbons soluble in CH_2Cl_2 were analyzed by dissolving 15 mg of a given fraction in 1 mL 15 % HF for 30-60 minutes. Organic compounds were then extracted in 0.8 mL CH_2Cl_2, and analyzed with an Agilent 6890 N/5793 MSD GC-MS equipped with an HP-5MS column (60 m, 0.25 mm i.d., stationary phase thickness 0.25 μm). C_2Cl_6 was employed as internal standard.

The total amount of oxidable hydrocarbons in the five fractions was determined using TGA. About 15 mg of sample was used, and heated to 650 with a heating rate of 5 °C/min. The final hold time at 650 °C was 2 h. The atmosphere was 4 mL/min O_2 + 8 mL/min N_2. The actual sample mass is plotted, and weight loss is given in percent of the mass of coke free sample.

The amounts of external and internal coke within the various catalyst fractions were estimated by combining the information from TGA and gas adsorption measurements [12,23]. TGA gives the total amount of coke (external + internal) and it is assumed that the reduction in micropore volume from the gas adsorption measurements relative to the fresh samples corresponds to the amount of internal coke, by assuming a coke density of 1.22 g/cm^3 [23]. The remaining amount of coke (found by subtraction) is then assumed to be external.

3. Results

3.1. Fresh catalysts

In this section, we will discuss the results obtained from basic characterization of the fresh unmodified ZSM-5 and desilicated D-ZSM-5 catalysts and their catalytic performance in the high pressure conversion of methanol to hydrocarbons.

3.1.1. Characterization of fresh catalysts

A full description of the characterization of the fresh catalysts is given in the supplementary information. These experiments show that the desilication leads to:

- Intact crystallinity, as inferred from XRD.
- A considerable decrease in Si/Al ratio, indicative of selective removal of framework silicon.
- Significant dissolution or etching along boundaries, intergrowths, and defects within each particle, as seen with SEM.
- A nitrogen isotherm displaying significant hysteresis resulting in significant mesoporosity evident from the BJH plot, a slightly increased BET surface area, and a fairly intact micropore volume.
- A mostly intact/slightly reduced concentration of Brønsted acid sites, as seen from the intensity of the ν(OH) bands at 3614 cm^{-1} in IR spectrum of the dehydrated samples and the band corresponding to protonated pyridine at 1554 cm^{-1}.
- Fairly extensive formation of Lewis acidity, as seen from the band at 1445-1442 cm^{-1} in the IR spectrum upon adsorption of pyridine.
- A significant introduction of weakly acidic sites (desorption of NH_3 below 350 °C), as seen from NH_3-TPD.
- A large increase in the concentration of isolated surface silanol groups, as seen from the band at 3745 cm^{-1} in the IR spectrum of the dehydrated sample, most likely corresponding to the mesopore surfaces.

Taken together, the characterization data show that the D-ZSM-5 catalyst is a representative desilicated catalyst [10,11,15,25]. The consequences of the changes in the acidic properties will be discussed in section 4.

3.1.2. Activity and product distribution in the MTH reaction at high pressure

The catalytic performance of the ZSM-5 and D-ZSM-5 samples was investigated in the high pressure conversion of methanol to hydrocarbons at 350 °C and 15 barg for a total reaction time of 160 h. No deactivation (as inferred from methanol breakthrough) was seen during these experiments. Product selectivities are given in Table 2 and a detailed analysis of the aromatics is shown in Figure 1. Notably, only a very small quantity of ethene is produced at elevated pressure. From the overall selectivities presented in Table 2, it appears that the general product distribution is not greatly affected by the desilication. However, the internal distribution of the methylbenzenes is strongly affected by desilication, and a clear shift towards heavier aromatics is observed (Figure 1). This is in line with previous reports and has been linked to changes in the diffusion properties of the catalysts as a consequence of mesopore formation [11].

Table 2. Normalized area of the outlet products (vol%) analyzed by GC after 160 h of reaction. C_1 = methane; C_2 = ethane + etene; C_3 = propane + propene

Catalyst	C_1	C_2	C_3	C_4	C_{5+}
ZSM-5	0.8	0.6	9.4	17.1	72.0
D-ZSM-5	1.0	0.5	7.3	14.4	76.8

It may be noted that the catalytic performance of a pair of ZSM-5 catalysts (parent and desilicated) prepared by following the same procedure as employed here has been reported previously [10]. Methanol was converted to hydrocarbon at elevated pressure also in the previous experiments, but the reaction was allowed to proceed to complete deactivation, thus allowing analysis of the activity data according to the model of Janssens [24]. It was found that the activity of the desilicated catalyst was reduced by a factor of 3 and that the rate of

deactivation decreased by a factor of 3.7, leading to an overall increase in conversion capacity by a factor of 3.6 for the desilicated catalyst [10]. Improvements in conversion capacity for desilicated catalysts appear to be a general observation [10,11,19,25,26,27]. Thus, significant differences in activity and rate of deactivation are expected also for the catalysts compared here. This point will be elaborated further in the discussion.

3.2. Analyses of fractions of deactivated catalysts

Subsequent to the catalytic test at high pressure, the reactor was cooled and the catalyst bed was carefully subdivided into several fractions. For ZSM-5, 10 such fractions were collected, whereas 5 fractions were selected for D-ZSM-5. These fractions are numbered consecutively from top to bottom of the catalyst beds. Due to the limited amounts of samples, not all fractions could be analyzed by all the techniques.

3.2.1. Quantification of coke and retained material by BET and TGA

The total amount of oxidable hydrocarbons on the partially deactivated fractions was determined using TGA. Data are listed in Tables 3 and 4 for ZSM-5 and D-ZSM-5, respectively. The full weight loss profiles from TGA are provided in the supplementary information.

Table 3. Various characterization of fresh and partially deactivated fractions of unmodified ZSM-5. TOS = 160 h.

Fraction of ZSM-5	Relative amount of soluble retained material (%)	Total amount of oxidable material from TGA (wt%)	Appx. temperature of oxidation (°C)	BET surface area (m^2/g)	Micropore volume[a] (cm^3/g)	Conversion of methanol; low pressure[b] (%)
Fresh	-	-	-	426	0.13	100
1	-	10.1	408	138	0.056	

2	100	3.9	430			43
3	-	1.65	420			
4	16	-	-	310	0.12	69
5	-	1.0	445			
6	12	-	-	309	0.13	65
7	-	1.3	430			
8	11	-	-	321	0.13	57
9	-	0.6	460			
10	15	0.5	460	321	0.13	66

[a]by t-plot method

[b]after 50 min on stream at $p_{methanol}$ = 130 mbar; WHSV = 5 $gg^{-1}h^{-1}$

Table 4. Various characterization of fresh and partially deactivated fractions of desilicated D-ZSM-5. TOS = 160 h.

Fraction of D-ZSM-5	Relative amount of soluble retained material (%)	Total amount of oxidable material from TGA (wt%)	Appx. temperature of oxidation (°C)	BET surface area (m^2/g)	Micropore volume[a] (cm^3/g)	Conversion of methanol; low pressure[b] (%)
Fresh	-	-	-	482	0.11	100
1	100	4.8	N/A[c]	367	0.087	100
2	95	4.8	270	368	0.098	82
3	44	4.8	290	373	0.098	48
4	33	4.6	335	383	0.099	45
5	30	4.5	345	363	0.098	37

[a]by t-plot method

[b]after 50 min on stream at $p_{methanol}$ = 130 mbar; WHSV = 5 $gg^{-1}h^{-1}$

[c]no clear plateau discernible

For the fractions of the unmodified ZSM-5 sample, a substantial difference in total coke content is seen when comparing the topmost fraction to the lower fractions. The topmost fraction contains about 10 wt% coke, whereas a weight loss of less than 1 wt% is observed for the lower fractions. This is in striking contrast to the data obtained for the fractions of D-ZSM-5, for which virtually no difference in coke content is seen throughout the catalyst bed. All five fractions contain very close to the same amount of coke as determined by TGA, about 4.6 wt%

For all fractions of both catalysts, some weight loss is seen at moderate temperature, followed by a more or less well defined plateau before a final weight loss occurs. This plateau is better defined for the fractions collected from the bottom of the catalyst bed, in particular for the D-ZSM-5 fractions, which contain an appreciable amount of oxidable material. We approximate that the first weight loss is due primarily to the loss of adsorbed water, whereas the second weight loss is mostly associated to the oxidation of hydrocarbons (coke). Clearly, the temperature of the onset of the second weight loss increases substantially from top to bottom, indicating that heavier or more stable coke species are formed in the lower fractions of the catalyst beds. Also, the temperatures of the onset of oxidation are generally substantially higher for the fractions of unmodified ZSM-5. This might be related to the improved diffusion characteristics of the desilicated catalyst and/or reflect differences in the chemical nature of the coke species present in the two catalysts. It can be argued that both these effects can cause the oxidation to occur more readily. This observation could have substantial implication for an industrial MTG application. If indeed a more moderate regeneration procedure is sufficient for a desilicated catalyst, an improved resistance towards long term, irreversible deactivation, which is known to occur during deactivation cycles, might be expected.

The BET surface areas and micropore volumes are also listed in Tables 3 and 4. For the partially deactivated fractions of both catalysts, a reduction in BET surface area is always seen. For the topmost fraction of ZSM-5, both the surface area and the micropore volume are severely reduced, whereas the subsequent fractions submitted to analysis show only a moderate reduction in surface areas and largely unaltered micropore volumes. Notably, no distinguishable trend is seen in the surface areas or micropore volumes of these subsequent fractions. For D-ZSM-5, a similar and moderate reduction of surface area and micropore volume is seen for all fractions. No clear trend is seen, except for a slightly further reduced micropore volume for the topmost fraction. The nitrogen adsorption measurements have revealed a profound difference between the fractions of ZSM-5 and D-ZSM-5. For the unmodified ZSM-5 sample, the topmost part of the catalyst bed displays a strong reduction in both surface area and micropore volume, which might reasonably be related to the fairly large amount of oxidable material (as determined by TGA) present for this particular fraction. No similar feature is seen for the desilicated catalyst.

3.2.2. DRUV-Vis spectroscopy of the partially deactivated fractions.

Sample darkening due to coke formation during the MTH reaction is well known [22,29,30,32,28]. The evolution of coke species inside the pores is complex and difficult to distinguish from the active catalytic scaffold of the hydrocarbon pool mechanism, since active molecules eventually transform into species responsible for the catalyst deactivation, i.e. coke molecules characterized by large conjugated systems. These species are characterized by electronic transitions that fall in the UV-Visible range. A qualitative characterization these species, both those entrapped inside and/or those adsorbed on the external surfaces is provided by the DRUV-Vis spectra shown in Figure 2 in the 330-700 nm range, for a selection of ZSM-5 and D-ZSM-5 fractions (five main bed fractions). For all samples, strong

absorptions in the ultraviolet range extending into the major part of the visible region are seen. As already discussed in previous papers [29,30], these absorption can be ascribed to $\pi \rightarrow \pi^*$ electronic transitions of hydrocarbons with an extensive electronic delocalization. Following previous assignments [29,30], $\pi \rightarrow \pi^*$ electronic transitions of species characterized by an increasing number of conjugated double bonds were taken into account to explain bands developing in the ultraviolet region and extending to the visible range. The simple model of an electron in a box allows one to estimate the length of the chains (number of conjugated double bonds) on the basis of the positions of the corresponding absorption bands. In order to identify the oligomers formed in/on the zeolite on the basis of the positions of the observed peaks, it is important to recall that the optical properties, in terms of band position and intensity, are clearly different in the case of neutral and/or carbocationic species [31]. In particular, in a series of oligomers, those which are carbocations give rise to more intense bands, shifted to higher wavelength. In a previous publication, this was shown by dosing of NH_3, given that strongly basic NH_3 should interact with carbocationic species and neutralize them, and the components in the 500-400 nm range were indeed eroded, while the other features remained unperturbed [29].

In the present case, upon comparison of the 2 samples we observed quite different behavior, even if the trend in the series is similar: i) moving from top to bottom the amount of adsorbed species decreases, ii) in both cases top fractions are characterized by the larger amount of adsorbed species.

In the ZSM-5 fractions (Figure 2, left panel) all the samples are characterized by a well defined band with a maximum centered at 415 nm and a shoulder at 396 nm, emerging from broad absorption extending to around 550 nm. The intensity of this main band becomes extremely high in the case of the top fraction. At higher energy, moving towards ultraviolet region, all samples are characterized by unresolved absorptions. This behavior can be

explained by the presence of a large variety of molecules, all characterized by similar nuclearity but different structure. At lower energy, only the top fraction shows the presence of a significant amount of species characterized by higher nuclearity. At least two main contributions can be identified at about 460 and 530 nm. These observations suggest that we do not have a substantial change in the nuclearity of the species moving from top to bottom and that the formation of the heavy coke occurs mainly in the top fraction.

In the D-ZSM-5 fractions, the overall intensity of the bands is significantly higher compared to ZSM-5, extending into nearly all of the visible range in all the fractions and presenting some differences among them. The top fraction is characterized by well defined components at 350, 380, 420, 460 (weak) and a broad absorption with evidence of maxima at 507, 570, and 623 nm. Most of the features falling in the visible range are still present, even if less defined, in case of fraction number 2. The other three spectra shown, corresponding to middle, 4, and bottom fractions are similar to one another and are characterized by an extensive broad and intense absorption in the 330—440 nm range that becomes significantly weaker starting from 440 to the end of the visible range.

On the basis of previous results and literature data, we can assign the components at 396 and 415 nm (in the case of ZSM-5), 380 and 420 nm (in the case of D-ZSM-5) to methyl substituted aromatic species with carbocationic character. Similar assignment could be given to the minor component at 460 nm being associated to a slightly larger molecule [29]. Small changes in band position can be due to slightly different nuclearities and number of methyl substituents of the species. Components at lower energy can be assigned to the growth of coke molecules towards larger conjugated system that are most probably linear polyaromatic in character [32].

A comparison between the two set of data (D-ZSM-5 and ZSM-5), brings us to these considerations: i) the top fraction of D-ZSM-5 is characterized by a large variety of more well

defined species, compared to the ZSM-5 counterpart, both in the region of methylated small aromatics (3 well separated band, instead of a band with a single maximum and a shoulder) and in the range of larger molecules (above 500 nm); ii) for the two samples different coke-like hydrocarbon species are revealed by means of DRUV-Vis spectroscopy, with bigger coke-like species, absorbing at higher wavelength, more abundant in the case of D-ZSM-5; iii) in case of D-ZSM-5 spectra collected for the fractions below the top fraction, are characterized by less drastic changes, testifying a more gradual evolution of the catalyst along the catalyst bed. All these observations are in line with the idea that in D-ZSM-5 zeolite, the reaction area that moves through the reactor, from top to bottom, is much wider in case of D-ZSM-5 than in case of ZSM-5 (see below). In D-ZSM-5 coke is progressively formed both inside the pores and externally, while in case of ZSM-5 coke is mostly formed outside the catalyst particles.

3.2.3. DRIFT spectroscopy of the partially deactivated fractions.

To obtain additional structural information on the retained carbon species and their interaction with the zeolite framework, FTIR spectroscopy was performed on the same fractions of both samples. Due to the generally low transmission of coke containing samples in the MIR range, they were recorded in reflectance mode (DRIFT) in air, after dilution with KBr (1:1). The results are reported in Figure 3, left panel for ZSM-5 and right panel for D-ZSM-5. To enable a quantitative comparison, all spectra are normalized to the framework overtone modes of the samples (maxima centered at 2010, 1875 and 1702 cm^{-1}).

Looking at the ZSM-5 spectra from high to low wavenumbers, the hydroxyl region is characterized by a number of more or less discrete absorption bands. A weak component is visible at 3740 cm^{-1}, which indicates that a large amount of external surface silanols are consumed by adsorption of water and hydrocarbons. As a result of the relatively weak

interaction of these surface silanols with various molecules present, their absorption frequencies are shifted, resulting in an intense and complex absorption with maximum centered around 3620 cm^{-1}. A weaker and even broader absorption with maximum centered at around 3215 cm^{-1}, is tentatively assigned to acidic hydroxyls which are more strongly hydrogen-bonded to entrapped species and consequently red shifted by ~300 cm^{-1}. In the 3000-2830 cm^{-1} range, aliphatic ν(CH) stretching modes are present, proving the presence of methylated and branched hydrocarbons. No evidence of aromatic CH species is observed, most likely due to their lower intensity in comparison with the aliphatic ones and to the overlap with the hydrogen bonded hydroxyls. The corresponding C=C stretching and C-H bending vibrational modes of the hydrocarbon molecules interacting with the hydroxyl groups of the zeolite give rise to bands in the region 1750-1350 cm^{-1} and indicate the formation of polyolefins and/or aromatics, among which are methyl-substituted benzene rings. Unfortunately, the assignments are somewhat hampered by overlap of signals corresponding to the zeolite framework overtones (1702 cm^{-1}) and the bending mode of physisorbed water (1630 cm^{-1}). In particular, the band at 1705 cm^{-1} can be associated to vibrations of tetrasubstituted C=C in olefinic compounds, while the bands in the 1630-1610 cm^{-1} range have been assigned to ν(C=C) stretching modes of a mixture of carbonaceous, hydrogen-deficient, species. Again, the bands at 1572 cm^{-1} and 1532 cm^{-1} can be due to ν(C=C) stretching modes in conjugated polyenes or aromatic species. Finally in the 1480-1370 cm^{-1} region, the bending vibrations of C-H in paraffinic (e.g. methyl substituents of aromatic compounds) and olefinic compounds are present [33,34,35].

By looking at the trend from top to bottom, a progressive decrease of the features ascribable to hydrogen-rich species (bands at 1705 cm^{-1} and in the 1480-1370 cm^{-1} range) in favor of hydrogen-deficient (coke-like) ones (bands in the 1630-1610 cm^{-1} range) is evident. All the spectra show a similar trend in the range 3650-3000. In particular, the component

associated to weakly perturbed hydroxyls (maximum around 3620 cm^{-1}) is always more intense relative to the band associated with more strongly perturbed hydroxyls (band centered at 3215 cm^{-1}). Moreover, this second maximum is significantly less intense along the series from top to bottom. This behavior is compatible with the fact that in the ZSM-5 sample, we do not observe an extensive formation of large hydrocarbon with extensive delocalized charge entrapped inside the cavities that would interact with and perturb available surface protons.

For the D-ZSM-5 fractions (Figure 3, right panel), the spectra look significantly different from those of the ZSM-5 fractions. The bands associated with hydroxyl groups, both isolated (band at 3740 cm^{-1}) and interacting (broad features in the 3720-2450 cm^{-1} range, with two maxima at 3600 and 3250 cm^{-1}) are much more pronounced suggesting a larger contribution of weakly perturbed water. The components associated to the stretching of -CH_n groups (3000-2830 cm^{-1} range) are much less intense than those observed in ZSM-5 case and they have the same abundance through the fractions. At lower frequencies the main features, beside the overtones of framework modes, can be identified at 1621, 1585, 1480, 1450 and 1397 cm^{-1}. By considering the strong intensity of the bands in the hydroxyl group range, the feature at 1621 cm^{-1} can be identified as the bending mode of water adsorbed in the D-ZSM-5 pores. It is worth noting that the top fraction seems to contain a larger quantity of water. The other bands can be assigned to ν(C=C) stretching modes (1585 cm^{-1}) and δ(C-H) bending modes (1480, 1450 and 1397 cm^{-1}) of the same species previously discussed in the case of ZSM-5 sample.

To summarize, in ZSM-5, the topmost fractions show the highest amount of methylated or branched hydrocarbons, while the lower ones reveal a consistent presence of coke-like species. On the contrary, D-ZSM-5 is consistent through the series of fractions and the overall intensities of the bands associated with the adsorbed species are lower. This is due

to the fact that IR bands from polycyclic species are less intense than those of aliphatic CH groups, which are more abundant in the case of ZSM-5.

3.2.4. Analysis of retained material by HF dissolution and extraction

Several fractions of partially deactivated catalyst were dissolved in hydrofluoric acid (HF), liberating retained hydrocarbons for extraction with CH_2Cl_2 and subsequent extract analysis by GC-MS. The composition and abundance of the retained hydrocarbons soluble in CH_2Cl_2 from the various fractions of the two catalysts are shown as total ion chromatograms in Figures 4 and 5. Operating at elevated pressure introduces additional complexity in the experimental set-up. Consequently, for several fractions of both catalysts, compounds not usually associated with reaction intermediates or coke formed in the methanol to hydrocarbons reaction are seen. For ZSM-5, significant amounts of diethylphthalate are found. This compound is commonly used as a plastic softener, and is not considered to be relevant to the MTH reaction. However, this contaminant might affect the characterization of the deactivated fractions by other techniques. Also, for the D-ZSM-5 sample, two unexpected compounds are detected. These were identified by high mass resolution GC-MS, and the $C_{11}H_{18}O$ species is believed to be an oxidation product formed during cooling of the catalyst, whereas the $C_{22}H_{30}$ compound is likely to be formed as a condensation product of this compound and other retained species (see supplementary information for details). Thus, for D-ZSM-5, the unexpected compounds are derived from the material actually retained during the MTH reaction, but have undergone further transformations unrelated to the MTH reaction. With these reservations in mind, it can be seen that for both samples, methyl benzenes ranging from toluene to hexamethyl benzene are the dominant species, in agreement with previous reports for samples investigated at low pressure [36,37]. One clear exception is seen for fraction 2 of the ZSM-5 sample, for which uncommonly high amounts of methyl substituted

naphthalenes are also seen. This might be a result of the high methanol pressure employed in the catalytic test. Clearly, fraction 2 of ZSM-5 (which is the topmost fraction analyzed) contains considerably more soluble retained material than the subsequent fractions, which are quite comparable with one another. Notably, very little penta- and hexamethyl benzene is found for these fractions and the xylenes are the most prominent single compounds.

Substantial variations are also seen among the fractions for the D-ZSM-5 sample. Clearly, there are large variations between the samples. For fraction 1, the $C_{22}H_{30}$ species and the oxygen containing $C_{11}H_{16}O$ species, which are believed to be formed from the most substituted methyl benzenes during cooling, are the most abundant single compounds, but these species decline rapidly upon passing down the catalyst bed. For the second fraction, the methyl benzenes, tetra- and hexamethyl benzene in particular, increase at the expense of the $C_{22}H_{30}$ and $C_{11}H_{16}O$ species. For the lower fractions, further reduction in the concentration of soluble retained material is seen.

To summarize, for both catalysts there is a distinct change when going from the top layers to the lower layers. The concentration of soluble retained hydrocarbons decreases from top to bottom. It is possible to estimate the relative amounts of soluble retained hydrocarbons based on the GC-MS analyses. Simple scrutiny of the chromatograms suggests that there is more soluble coke in the top fractions, and this is confirmed by the more quantitative analysis given in Tables 3 and 4, where results from TGA are also included. Unfortunately, accurate quantitative analyses of the amount of soluble retained material are not available, due to difficulties in obtaining an accurate calibration for such a wide variety of compounds. Also, the dissolution/extraction approach only allows detection of species heavier than benzene, meaning that adsorbed methanol/DME, methoxy groups, and trapped alkanes are not accounted for. Thus, the data in Tables 3 and 4 are given relative to the topmost fraction analyzed for both catalysts.

3.2.5. Catalytic activity of partially deactivated catalyst fractions

For both ZSM-5 and D-ZSM-5, selected fractions were tested for catalytic activity in the conversion of methanol to hydrocarbons, in order to investigate relative deactivation down the bed. The results for the parent ZSM-5 catalyst and the desilicated D-ZSM-5 catalyst are given in Figures 6 and 7, respectively. Activities are also listed in Tables 3 and 4. For ZSM-5, all fractions display a methanol conversion which is lower than 100 %. Further, the topmost fraction appears to be significantly more deactivated than the lower fractions, for which the activities are comparable. When tested at the same reaction conditions, the parent ZSM-5 sample converts 100 % of the methanol, meaning that all the fractions are substantially deactivated. The product selectivities are as expected, and are nearly identical for all fractions (see also below).

The results obtained for the fractions of the D-ZSM-5 catalyst are very different, as seen in Figure 7, especially considering the changes in activity when going down the bed. In the desilicated sampled there is a clear decrease in activity when going down the bed, starting with full conversion in the top fraction and going down to less than 40 % conversion in the bottom fraction. This is in stark contrast to the results obtained for the parent ZSM-5, which displays lower activity at the top layer compared to the layers going down the bed. It is noteworthy that the topmost fraction of D-ZSM-5 has retained a comparatively high activity. For the fractions of the D-ZSM-5 catalyst, significant differences in product selectivities are also seen. Clearly, as the level of conversion decreases, the selectivity towards C_{6+} decreases while that of C_3 products increases. Also, the C_3/C_2 ratio increases with deactivation down the bed. This observation is rather unspectacular, as the results are in very close agreement with the conversion-selectivity relations generally observed for ZSM-5 catalysts [38]. As a final remark, it can be noted that at the same level of conversion, e.g. by comparison of the topmost

fraction of ZSM-5 and the second-to-last fraction of D-ZSM-5, the desilicated sample tends to yield less C_2 and more C_{6+} and butanes, in agreement with previous reports [11].

The catalytic tests of the individual fractions of the parent and desilicated catalysts have revealed profound differences in the deactivation behavior as a function of the axial position in the catalyst bed. For the ZSM-5 sample, the topmost fraction is more severely deactivated than the others, which display nearly identical activities. In contrast to this, the D-ZSM-5 sample is increasingly more deactivated when passing from the top to the bottom fractions.

4. Discussion

The objective of this discussion is twofold. First, an unusually large and varied number of techniques have been employed to investigate the partially deactivated zeolite catalyst fractions. Thus, from a methodological perspective it is worthwhile to evaluate to which extent these analysis techniques give comparable results and insights and to which extent they provide complementary information. Second, a key objective will of course be to compare the untreated and the desilicated ZSM-5 catalysts in an attempt to pinpoint the underlying phenomena leading to the improved deactivation resistance previously demonstrated for desilicated zeolites [10,11]. As a general feature, it should be mentioned that these discussions will be somewhat complicated by the fact that not all catalyst fractions have been analyzed with every technique. Consequently, emphasis will be placed on the trends observed when comparing fractions axially downwards in the catalyst bed. To facilitate this discussion, the results from the quantitative analysis techniques have been compiled in a graphical manner in Figure 8.

We will first consider the information available regarding the total quantity of hydrocarbons deposited on the parent ZSM-5 catalyst. Thermogravimetric analysis unequivocally shows that there is a very substantial decrease in the total amount of oxidable material (the second, high temperature weight loss not associated with water desorption) when going from top to bottom. In apparent agreement, the BET surface area and micropore volume are also severely reduced for the topmost sample submitted to analysis by nitrogen adsorption. Similarly, the intensities of the general features from DRUV-Vis and FTIR spectroscopy indicate that, for ZSM-5, there is gradually less material deposited downwards in the catalyst bed. Turning now to the information regarding the chemical nature of the deposits on the parent ZSM-5 catalyst, it seems clear that the estimated temperature of the onset of oxidation increases from top to bottom. The percentage of retained hydrocarbons amenable to GC-MS analysis (soluble in CH_2Cl_2) decreases from top to bottom, and this decrease is larger than the decrease in overall coke content from TGA. Both these observations indicate that the hydrocarbons deposited on the catalyst become increasingly heavy down the bed. Also, considering the ratio between the intensities of the signals corresponding to aliphatic ν(CH) stretching modes and aromatic ν(CC) stretching modes, the FTIR suggests an increased degree of condensation (heavier species) when going from top to bottom. Finally, the intense band seen at 415 nm seen in the DRUV-Vis spectra assigned to the comparatively light cationic methylbenzenes decreases from top to bottom, in particular when comparing the topmost and the subsequent fractions. Briefly, for ZSM-5 it may be stated that taken together, these analyses show that when moving axially down the catalyst bed; 1) the total amount of deposited hydrocarbons decrease, and 2) the hydrocarbons deposited become heavier and/or more condensed, although this latter observation is not evident in the DRUV-Vis spectra.

For the desilicated D-ZSM-5 catalyst, thermogravimetry conveys a different impression; there is no significant difference in the total amount of deposited material among

the fractions. Nitrogen adsorption appears to agree, the BET surface areas and micropore volumes are similar for all fractions, except a slightly smaller micropore volume for the top fraction. The DRUV-Vis spectra might indicate a reduction in the amount of hydrocarbons deposited when going from top to bottom; in particular the top fraction appears to stand out. FTIR, on the other hand, does not reveal any major differences in the total amount of deposited material with respect to axial bed position. As for the parent sample, both the temperatures of the onset of oxidation (which are more accurately determined for these fractions, given the similar coke content) and the total integrated intensities of the GC-MS chromatograms show that the species retained on the catalyst also become increasingly heavy/more condensed for the desilicated catalyst. However, this trend is not easily discernible using FTIR for D-ZSM-5. As mentioned above, the DRUV-Vis spectra suggest that the deposits are more complex for the top fraction. The results from the various analysis methods are somewhat harder to reconcile for the D-ZSM-5 fractions; however, a general picture emerges; 1) there are no major differences or trends in the total amount of deposited hydrocarbons along the catalyst bed; 2) the deposits appear to become heavier and/or more condensed when going from top to bottom.

We now turn to a comparison of the modes of deactivation for the two catalysts. For the fractions of ZSM-5 catalyst, the atmospheric pressure catalytic tests show a lower residual activity for the topmost fraction (actually fraction 2) tested and no significant differences for the subsequent catalyst fractions. As described in the discussion above, the top fractions contain a large total amount of coke (TGA), and a severe reduction of surface area and micropore volume is seen for the topmost fraction. These features are easily reconciled with a high degree of deactivation and low residual activity. It is, however, somewhat unexpected that the further reductions in total coke content and shifts towards heavier coke further down in the bed do not result in any trend in the residual activity. It might be that these two effects

counterbalance each other; one could reasonably assume that less coke corresponds to less deactivation whereas heavier coke species are more efficient in deactivating the catalyst. Schulz [22] has investigated the MTH reaction over ZSM-5 at 475 °C and describes the deactivation phenomena occuring axially downwards in the reactor bed: An initial heavily deactivated black zone of catalyst (with coke on the external surface) is followed by a grey reaction zone (where most of the methanol is converted) and finally a less deactivated light-blue zone (where some coke seeds have been formed in secondary reactions of the MTH products). It is further suggested that the (grey) reaction zone migrates slowly along the catalyst bed during the catalyst lifetime [22]. A similar description of catalyst deactivation in a plug flow reactor has been given by Haw and Marcus for H-SAPO-34 and was referred to as a "cigar burn" time evolution of the catalyst bed [39]. Our observations for the parent ZSM-5 catalyst are in agreement with these findings; the most profound build up of coke first occurs in the topmost layers of catalyst.

For the mesoporous D-ZSM-5 catalyst, as already pointed out, the axial residual activity profile is quite different. The top fraction displays 100 % methanol conversion, whereas significant reductions in residual activity are seen for the second and third fractions. This trend appears to continue for the fourth and fifth fractions; however, these reductions are comparatively small and might not be significant. The total coke content is virtually identical for all fractions, and cannot play a major role. However, the trend in residual activity might be associated with the observed tendency for the coke species to become heavier and/or more condensed when going from top to bottom for the D-ZSM-5 catalyst; provided that the heavier coke species are more efficient in deactivating the catalyst, as speculated above.

It is well established that mesoporous, desilicated ZSM-5 catalysts display improved lifetime or resistance towards deactivation in the MTH reaction [10,11,12,13]. It has previously been suggested that deactivation of ZSM-5 catalysts is dominated by the formation

of coke, possibly graphitic, on the external surface of the crystallites [22,36,40]. This is in contrast to catalysts such as zeolite beta and SAPO-34, for which it has been shown that deactivation is closely related to the build up of trapped polyaromatics within the voids of the porous structures [22,41,42,43,44]. Thus, our initial hypothesis was that the desilicated sample would be more resistant towards deactivation due to a higher tolerance for external coke caused by the effectively higher external surface of each individual crystal as a consequence of mesopore formation after desilication. This notion is examined further in Figure 9, where the coke deposits are subdivided into internal and external coke, based on the combined information from thermogravimetric and gas adsorption measurements. Clearly, this hypothesis does not provide a fully satisfactory explanation for the differences in residual activity when comparing the two catalysts. The top fraction of D-ZSM-5 contains the smallest amount of external coke and displays the highest residual activity, seemingly in agreement with this theory. However, for the most deactivated top fraction of untreated ZSM-5, the amount of *internal* coke is extreme. This indicates that internal coke might also play a role in the deactivation of the catalyst. Further, Figure 9 very clearly shows that the desilicated catalyst accommodates a much larger amount of external coke than the parent catalyst. Both these points indicate that desilication does indeed affect the distribution of coke deposits (external versus internal). At this point, it should be mentioned that a discussion based solely on a subdivision into internal and external coke is likely to be an oversimplification. In a recent study on a large number of desilicated and untreated catalysts, it was found that the deactivation rate correlated with the *ratio* between internal and external silanol groups [20], indicating that a more refined analysis might be appropriate. Nevertheless, the most obvious difference between the two samples examined here is seen for the axial distribution of the total coke content along the catalyst bed. It is tempting to link the more even distribution of coke among the fractions of D-ZSM-5 to an increased mobility of coke and coke precursors

for the desilicated catalyst, suggesting that *porosity* plays an important role for the improved deactivation behavior of the desilicated catalyst, as also suggested previously [11,13].

However, the observed difference in the axial distribution of the total coke could also be attributed to differences in *activity* between the catalysts. The characterization data presented above reveal significant alterations in the acidic properties upon desilication. Clearly, a very active catalyst will convert all the methanol into hydrocarbons (and coke) in the topmost layers of the catalyst bed, leaving the bottommost layers to catalyze mainly secondary reactions, as described by Schultz [22]. On the other hand, for a catalyst having lower activity, which, as mentioned in section 3.1.2., is expected for the desilicated catalyst [10], a larger fraction of the catalyst is required to convert the methanol. Thus, we speculate that a less active catalyst will have a longer reaction zone, or "cigar burn" zone, in the terminology of Haw and Marcus mentioned above [39], and therefore also possibly constitute a system with less pronounced gradients. This notion is summarized in Figure 10, where we illustrate that differences in activity (as well as porosity) are likely to contribute to the variations observed when comparing the parent and the desilicated ZSM-5 catalysts.

5. Conclusions

Previous literature reports have established that desilicated zeolite catalysts display improved lifetime or resistance towards deactivation in hydrocarbon transformation processes involving coking. We have investigated a desilicated (D-ZSM-5) and a non-desilicated (ZSM-5) catalyst that were partially deactivated in the conversion of methanol to hydrocarbons at elevated reaction pressure. The catalyst beds were fractionated from top to bottom, and these fractions were analyzed by a variety of characterization techniques to investigate the deactivation phenomena. The results presented in this contribution have revealed profound

differences when comparing the deactivation behavior of desilicated and regular, non-treated ZSM-5 catalysts, and several observations are made.

- The parent catalyst displays a substantial gradient in the total coke content axially along the catalyst bed; much more coke is deposited in the topmost layers of the catalyst bed.
- On the contrary, the desilicated catalyst displays a much more homogeneous coke distribution; all catalyst fractions contain the same amount of hydrocarbon deposits.
- The desilicated catalyst accommodates more external coke than the parent sample.
- For both catalysts, there appears to be a shift towards heavier or more condensed coke species when going from top to bottom of the catalyst bed.
- The temperature of the onset of oxidation of hydrocarbon deposits is overall lower by at least 100 °C for the desilicated zeolite, indicating that milder regeneration conditions might be sufficient for the desilicated catalyst.
- Measurements of the residual activity of the fractions of the two catalysts show substantial differences. The parent catalyst appears to be most severely deactivated at the top of the catalyst bed, and no significant differences are seen when comparing the subsequent fractions. However, for the desilicated catalyst, the bottommost fractions are more severely deactivated than the top fractions.

It is clear that the (axial) mode of catalyst deactivation and the chemical nature of the carbonaceous species are substantially influenced by the desilication procedure, which alters not only the catalyst *porosity* but also the catalyst *activity* and *rate of deactivation*. Unfortunately, we are not (yet) at a position where we fully can understand (and predict) the deactivation resistance of zeolite catalysts. However, a clear strategy to move closer to reaching this objective has emerged, based on fractionation/characterization procedures described here. As a path for further work, we suggest to perform similarly detailed analyses

for a *series of increasingly deactivated catalyst samples* obtained in catalytic testing at realistic conditions. This will provide information about the entire deactivation process, from fresh to fully deactivated catalyst, beyond the two instantaneous snapshots presented here. Moreover, the very rewarding and detailed information from ex-situ measurements should be complemented by in-situ or in-operando measurements allowing spatial mappings, as described in very recent literature [32,45,46,47].

Acknowledgements

This publication forms a part of the inGAP Center of Research based Innovation, which receives financial support from the Research Council of Norway under contract no. 174893. We acknowledge Prof. Einar Uggerud and Dr. Osamu Sekiguchi at the mass spectrometry laboratory at the Department of Chemistry, University of Oslo for performing the high mass resolution GC-MS analyses.

Figure captions

Figure 1. Normalized distribution of methyl benzenes in the effluent after 160 h of methanol conversion over the parent ZSM-5 and the desilicated D-ZSM-5 counterpart. WHSV= 0.75 $gg^{-1}h^{-1}$, reaction temperature= 350 °C, total pressure 15 barg.

Figure 2. DRUV-Vis spectra of the fractions in ZSM-5 (left) and D-ZSM-5 (right) runs. TOS = 160 h; sample exposed to laboratory air.

Figure 3. DRIFT spectra of the fractions in air in ZSM-5 (left) and D-ZSM-5 (right) runs. TOS = 160 h; sample exposed to laboratory air.

Figure 4. Chromatograms showing retained hydrocarbons soluble in CH_2Cl_2 for the various fractions of ZSM-5. TOS = 160 h. * indicates the position of the internal standard C_2Cl_6 and × diethyl phthalate.

Figure 5. Chromatograms showing retained hydrocarbons soluble in CH_2Cl_2 for the various fractions of D-ZSM-5. TOS = 160 h. * indicates the position of the internal standard C_2Cl_6. The origin of the $C_{11}H_{16}O$ and $C_{22}H_{30}$ species is discussed in the text.

Figure 6. Conversion of methanol over partially deactivated fractions of the parent ZSM-5 catalyst. The experiments were carried out at low pressure (p_{MeOH} = 130 mbar), reaction temperature 350 °C and WHSV = 5 $gg^{-1}h^{-1}$. Black squares indicate conversion level after 50 minutes on stream for each fraction and the bars the distribution (C%) of products.

Figure 7. Conversion of methanol over the fractions in the desilicated D-ZSM-5 catalyst. The experiments were carried out at low pressure (p_{MeOH} = 130 mbar), reaction temperature 350 °C and WHSV = 5 $gg^{-1}h^{-1}$. Black squares indicate conversion level after 50 minutes on stream for each fraction and the bars the distribution (C%) of products.

Figure 8. Summary of results from the quantitative characterization techniques employed for the partially deactivated catalyst fractions of the parent ZSM-5 (left) and the desilicated D-ZSM-5 (right) catalysts. TOS = 160 h.

Figure 9. The distribution of the total (black), internal (dark grey) and external (pale grey) amount of coke in the different fractions of the unmodified ZSM-5 (left) and desilicated D-ZSM-5 (right) catalysts. TOS = 160 h. Total coke was measured by TGA, assuming that the weight loss of deactivated fractions is entirely due to coke combustion. The internal amount of coke is calculated by decrease in micropore volume of the deactivated fractions respect to the corresponding fresh mother sample as determined by the t-plot method. The external coke is calculated from difference of the two.

Figure 10. Schematic of coke distribution in the reactors (left) and methanol concentration profiles axially along the reactors (right) for the parent (top) and desilicated (bottom) catalysts. The desilicated catalyst is less active and will have a wider reaction zone, leading to a more even build up of coke, as indicated by the shading of the catalyst particles. Also, the parent catalyst is more prone to external coking towards the bottom of the catalyst bed, indicated by the black line defining the circumference of the particles.

References

[1] W. Vermeiren, J.P. Gilson, Top. Catal. 52 (2009) 1131.

[2] U. Olsbye, S. Svelle, M. Bjørgen, P. Beato, T. Janssons, F. Joensen, S. Bordiga, K. P. Lillerud, Angew. Chem. Int. Ed. 51 (2012) 2.

[3] S. Svelle F. Joensen, U. Olsbye, K.-P. Lillerud, M. Bjørgen, J. Phys. Chem. C, 111 (2007) 17981.

[4] M. Bjørgen, F. Joensen, K.P. Lillerud, U. Olsbye, S. Svelle, Catal. Today, 142 (2009) 90.

[5] S. Teketel, U. Olsbye, K.P Lillerud, P. Beato, S. Svelle, Microporous Mesoporous Mater. 136 (2010) 33.

[6] F. Bleken, W. Skistad, K. Barbera, M. Kustova, S. Bordiga, P. Beato, K. P. Lillerud, S. Svelle, U. Olsbye, Phys. Chem. Chem. Phys. 13 (2011) 2539.

[7] L.R. Aramburo, E. de Smit, B. Arstad, M.M. van Schooneveld, M. Matti L. Sommer, A. Juhin, T. Yokosawa, H.W. Zandbergen, U. Olsbye, F.M.F. de Groot, B.M. Weckhuysen, Angew. Chem. Int. Ed. 51 (2012) 3616.

[8] L. Karwacki, D.A.M. de Winter, L.R. Aramburo, M.N. Lebbink, J.A. Post, M.R. Drury, B.M. Weckhuysen, Angew. Chem. Int. Ed. 50 (2011) 1294.

[9] S. Malola, S. Svelle, F. Bleken, O. Swang, Angew. Chem. Int. Ed. 51 (2012) 652.

[10] S. Svelle, L. Sommer, K. Barbera, P. N. R. Vennestrøm, U. Olsbye, K. P. Lillerud, S. Bordiga, Y.-H. Pan, P. Beato, Catal. Today 168 (2011) 38.

[11] M. Bjørgen, F. Joensen, M. Spangsberg Holm, U. Olsbye, K.-P. Lillerud, S. Svelle, Appl. Catal. A 345 (2008) 43.

[12] M. Choi, K. Na, J. Kim, Y. Sakamoto, O. Terasaki, R. Ryoo, Nature 461 (2009) 246.

[13] J. Kim, M. Choi, R. Ryoo, J. Catal. 269 (2010) 219.

[14] M. Hartmann, Angew. Chem. Int. Ed. 43 (2004) 5880.

[15] J. Perez-Ramirez, C.H. Christensen, K. Egeblad, C.H. Christensen, J.C. Groen, Chem. Soc. Rev. 37 (2008) 2530.

[16] K. Egeblad, C.H. Christensen, M. Kustova, C.H. Christensen, Chem. Mater. 20 (2008) 946.

[17] R. Chal, C. Grardin, M. Bulut, S. van Donk, ChemCatChem 3 (2011) 67.

[18] S. van Donk, A.H. Janssen, J.H. Bitter, K.P. de Jong, Catal. Rev. Sci. Eng. 45 (2003) 297.

[19] D. Verboekend, J. Perez-Ramirez, Catal. Sci. Technol. 1 (2011) 879.

[20] K. Barbera, F. Bonino, S. Bordiga, T.V.W. Janssens, P. Beato, J. Catal. 280 (2011) 195.

[21] P. Sazama, B. Wichterlova, J. Dedecek, Z. Tvaruzkova, Z. Musilova, L. Palumbo, S. Sklenak, O. Gonsiorova, Microporous Mesoporous Mater. 143 (2011) 87.

[22] H. Schultz, Catal. Today 154 (2010) 183.

[23] D.M. Bibby, C.G. Pope, J. Catal. 116 (1989) 407.

[24] T.V.W. Janssens, J. Catal. 264 (2009) 130.

[25] F. Schmidt, M.R. Lohe, B. Buchner, F. Giordanino, F. Bonino, S. Kaskel, Microporous Mesoporous Mater. 165 (2012) 148.

[26] M. Spangsberg Holm, E. Taarning, K. Egeblad, C. Hviid Christensen, Catal. Today 168 (2011) 3.

[27] A.A. Rownaghi, F. Rezaei, J. Hedlund, Microporous Mesoporous Mater. 151 (2012) 26.

[28] D. Mores, E. Stavitski, M.H.F. Kox, J. Kornatowski, U. Olsbye, B.M. Weckhuysen, Chem. Eur. J. 14 (2008) 11320.

[29] L. Palumbo, F. Bonino, P. Beato, M. Bjørgen, A. Zecchina, S. Bordiga, J. Phys. Chem. C 112 (2008) 9710.

[30] M. Bjørgen, F. Bonino, S. Kolboe, K.P. Lillerud, A. Zecchina, S. Bordiga, J. Am. Chem. Soc. 125 (2003) 15863.

[31] S. Bordiga, G. Ricchiardi, G. Spoto, D. Scarano, L. Carnelli, A. Zecchina, C.O. Arean, J. Chem. Soc., Faraday Trans. 89 (1993) 1843.

[32] D. Mores, J. Kornatowski, U. Olsbye, B.M. Weckhuysen, Chem. Eur. J. 17 (2011) 2874.

[33] M. Rozwadowski, M. Lezanska, J. Wloch, K. Erdmann, R. Golembiewski, K. Kornatowski, J. Chem. Mater. 13 (2001) 1609.

[34] H.G. Karge, W. Niessen, H. Bludau, Appl. Catal. A 146 (1996) 339.

[35] D. Meloni, D. Martin, P. Ayrault, M. Guisnet, Catal. Lett. 71 (2001) 213.

[36] M. Bjørgen, S. Svelle, F. Joensen, J. Nerlov, S. Kolboe, F. Bonino, L. Palumbo, S. Bordiga, K.-P. Lillerud, U. Olsbye, J. Catal. 249 (2007) 195.

[37] S. Svelle, F. Joensen, J. Nerlov, U. Olsbye, K.-P. Lillerud, S. Kolboe, M. Bjørgen, J. Am. Chem. Soc. 128 (2006) 14770.

[38] C.D. Chang, Catal. Rev. Sci. Eng. 25 (1983) 1.

[39] J.F. Haw, D.M. Marcus, Top. Catal. 34 (2005) 41.

[40] D. Mores, E. Stavitski, M.H.F. Kox, J. Kornatowski, U. Olsbye, B.M. Weckhuysen, Chem. Eur. J. 14 (2008) 11320.

[41] B.P.C. Hereijgers, F. Bleken, M. Hellner Nilsen, S. Svelle, M. Bjørgen, K.P. Lillerud, B.M. Weckhuysen, U. Olsbye, J. Catal. 264 (2009) 77.

[42] F. Bleken, M. Bjørgen, L. Palumbo, S. Bordiga, S. Svelle, K.P. Lillerud, U. Olsbye, Top. Catal. 52 (2009) 218.

[43] M. Bjørgen, U. Olsbye, S. Kolboe, J. Catal. 215 (2003) 30.

[44] M. Bjørgen, S. Akyalcin, U. Olsbye, S. Kolboe, S. Svelle, J. Catal. 275 (2010) 170.

[45] D.S. Wragg, D. Akporiaye, H. Fjellvåg, J. Catal. 279 (2011) 397.

[46] D.S. Wragg, R.E. Johnsen, M. Balasundaram, P. Norby, H. Fjellvåg, A. Grønvold, T. Fuglerud, J. Hafizovic, Ø.B. Vistad, D. Akporiaye, J. Catal. 268 (2009) 290.

[47] Y.-M. Chung, D. Mores, B.M. Weckhuysen, Appl. Catal. A 404 (2011) 12.

Supporting information for:

Catalyst deactivation by coke formation in microporous and desilicated zeolite H-ZSM-5 during the conversion of methanol to hydrocarbons

Francesca Lønstad Bleken[1], Katia Barbera[2], Francesca Bonino[3], Unni Olsbye[1], Karl Petter Lillerud[1], Silvia Bordiga[3,*], Pablo Beato[4,*] Ton V. W. Janssens[4], Stian Svelle[1,*]

[1] inGAP Center of Research Based Innovation/Center for Materials Science and Nanotechnology (SMN), University of Oslo, Department of Chemistry, N-0315 Oslo, Norway

[2] Department of Industrial Chemistry and Materials Engineering, University of Messina V.le F. Stagno d'Alcontres 31, I-98166, Messina, Italy

[3] Department of Chemistry, NIS Centre of Excellence, and INSTM Centro di Riferimento University of Turin, Via Quarello 15, I-10135, Turin, Italy

[4] Haldor Topsøe, Nymøllevej 55, DK-2800 Kgs. Lyngby, Denmark

1. Characterization of fresh catalysts

The fresh parent and the fresh desilicated catalysts were characterized using a variety of methods prior to testing in the MTH reaction. Prior to presenting the characterization data, it should be mentioned that, due to limitations in sample amount, some of the characterization of the desilicated catalyst (elemental analysis by ICP-MS and pyridine adsorption followed by FTIR) had to be performed using a different batch of desilicated catalyst than the one employed in the catalytic testing. This batch was prepared from the same starting material according to exactly the same procedure, but as the reproducibility might not be perfect, we limit ourselves to a qualitative discussion of these characterization data. We are confident that the catalyst sample studied with XRD and pyridine is representative, and that the use of two different batches has no significant influence on the conclusions made.

Experimental

X-Ray Powder Diffraction patterns have been collected with a PW3050/60 X'Pert PRO MPD diffractometer from PANalytical working in Bragg-Brentano, using as source the high power ceramic tube PW3373/10 LFF with a Cu anode equipped with Ni filter to attenuate K_β Scattered photons have been collected by a RTMS (Real Time Multiple Strip) X'celerator detector. Powdered samples have been hosted on SiO_2 amorphous sample holder.

BET surface areas were determined by N_2 adsorption at -196 °C on an ASAP2020 Micromeritics instrument. Prior the measurements, the samples were outgassed at 150 °C overnight to release water. Different types of porosities were evaluated through the t-plot method (Harkins and Jura universal thickness curve).

Scanning electron microscopy (SEM) was done on a FEI XL30 FEG-SEM operating at 5-15 kV. SEM specimens were prepared by placing a small amount of sample powder on

carbon tape on SEM stubs. In order to minimize the charging issue, the samples were coated with ca. 12 nm thick Pd/Pt layer.

The acid site density of the materials was determined by temperature programmed desorption of ammonia (NH_3-TPD). The TPD profiles were monitored by thermogravimetric analysis (TGA), using a Mettler TG/DSC1 LF instrument. Between 40 and 60 mg sample was dried in N_2 at 500 °C for 2 h in a TGA crucible, and cooled to 150 °C. Ammonia was adsorbed at that temperature for about 30 min, using a mixture of 2% NH_3 in He (75 mL/min), and purged in pure N_2 (75 mL/min) for 4 h to remove all loosely bound NH_3, until no further weight changes were observed. The desorption of NH_3 was then monitored by the weight loss while increasing the temperature to 600 °C with 10 K/min in a flow of 75 mL/min N_2. An equivalent Si/Al ratio was calculated using the NH_3 adsorption capacity, assuming that one NH_3 molecule corresponds to one Al substitution.

The fresh catalysts were characterized by Fourier Transform InfraRed spectroscopy (FTIR) to monitor acidic site distribution from adsorption of CO and pyridine. The spectra were collected in transmission mode with a resolution of 2 cm^{-1} on a self-supporting pellet using a Nicolet 6700 FTIR spectrometer directly connected with a cryogenic cell to allow also thermal treatment in high vacuum. Samples were activated at 450 °C. For CO adsorption, samples were then cooled to -196 °C with 60 mbar CO dosage. Adsorption of pyridine was performed by exposing the pellets to the vapor pressure of pyridine at room temperature followed by evacuation at 150 °C. The spectra have been normalized to the overtone modes in the 1750–2100 cm^{-1} region.

Results

XRD patterns of the fresh catalysts are presented in Figure S.1. Clearly, both display show the diffraction pattern of the MFI structure. However, it can be noticed that a slight

broadening of the reflexes are observed for the desilicated catalyst. This might be linked to a reduction of the crystallite domain size upon desilication.

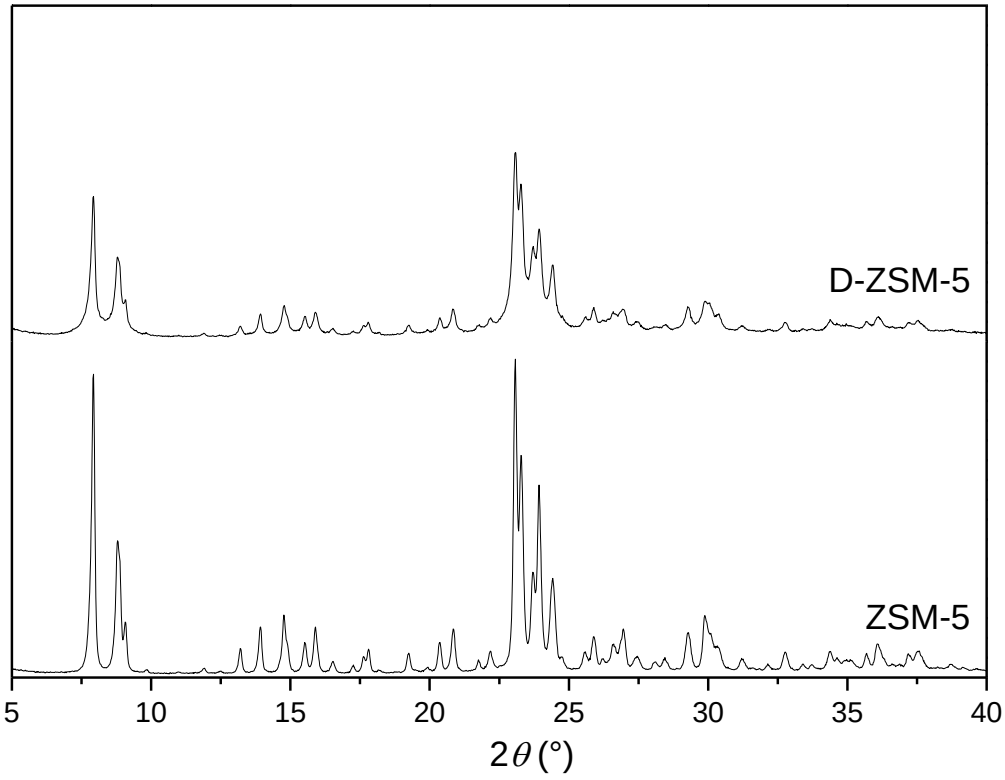

Figure S.1. XRD patterns of the fresh desilicated (top) and parent (bottom) catalysts.

Nitrogen adsorption isotherms are shown in Figure S.2., and surface area measurments are presented in Tables 3 and 4 of the main manuscript and repeated in Table S.1 below for convenience. Very clearly, the nitrogen isotherm for the desilicated sample displays significant hysterisis, indicative of mesoporosity, which is confirmed in the BJH-plot. The fresh desilicated sample displays a significantly higher surface area than the fresh unmodified catalyst and a fairly similar micropore volume (Table S.1). Such observations are well documented after desilication and are related to the creation of mesopores in the zeolite [1,2,3].

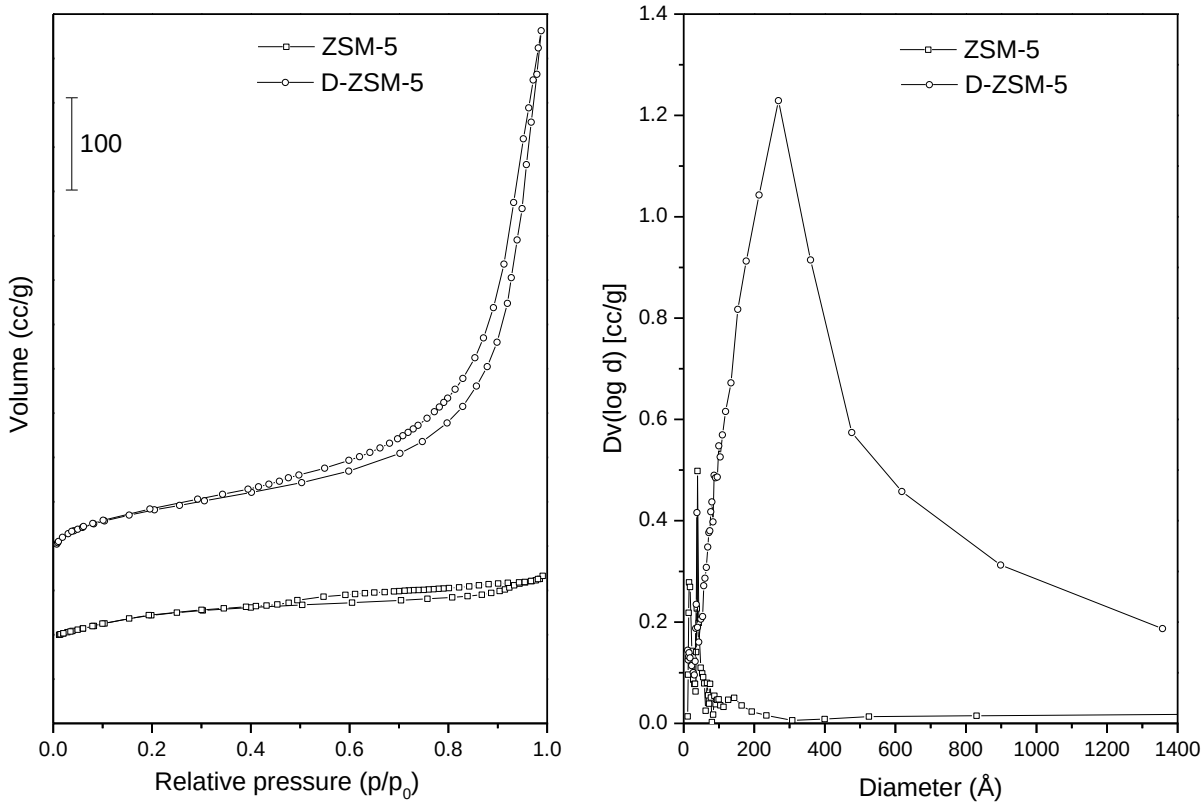

Figure S.2. Nitrogen adsorption isotherms (left) and BJH mesopore distribution from the desorption branch (right). The isotherms have been vertically shifted for clarity.

Table S.1. BET surface areas and micropore volumes from nitrogen adsorption.

Catalyst	BET surface area (m^2/g)	Micropore volume[a] (cm^3/g)
ZSM-5	426	0.13
D-ZSM-5	482	0.11

[a]by t-plot method

SEM images of the fresh ZSM-5 and D-ZSM-5 catalysts are shown in Figure S.3. Clearly, substantial dissolutions are seen for the desilicated catalyst, and it appears that the crystal dissolution has occured primarily along boundaries or defects within each particle upon according to the mode suggested by Ogura et al. [4].

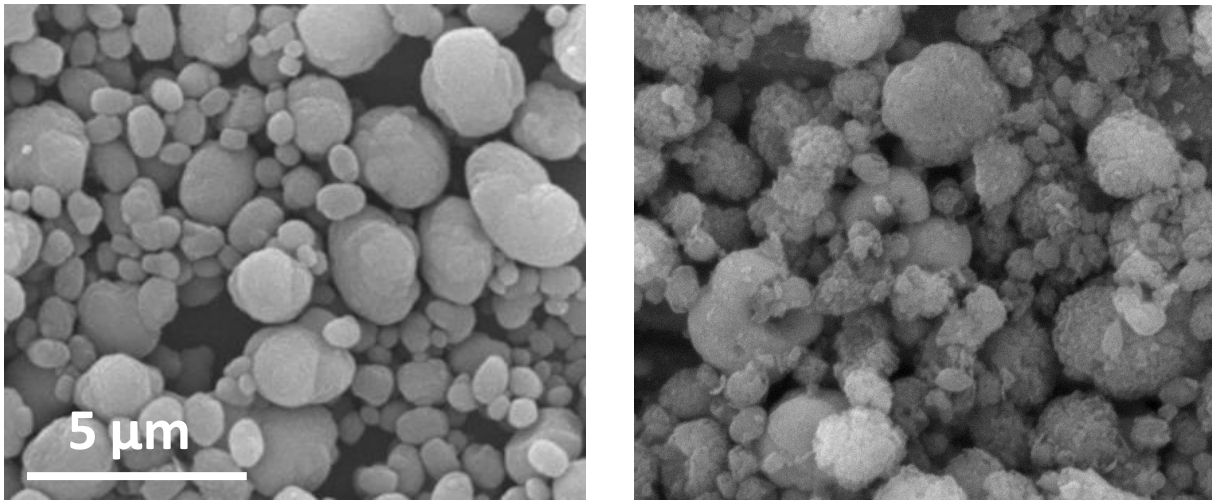

Figure S.3. SEM micrographs for the non-treated fresh ZSM-5 catalyst (left panel) and the fresh desilicated D-ZSM-5 catalyst (right panel).

Full NH_3-TPD profiles of both catalysts are given in Figure S.4, and a quantitative analysis of the desorption experiments is listed in Table S.2 together with the results of the elemental analysis. Clearly, desilication leads to a decrease in the Si/Al as determined by either method as a consequence of the selective removal of silicon. Inspection of the TPD profiles reveals that the distribution of acid sites also changes considerably upon desilication. It appears that desilication leads to a considerable formation of weaker acid sites, as evidenced by significant desorption at fairly low temperatures seen for the D-ZSM-5 catalyst. This is further emphasized in Table S.2, where the desorption has been subdivided (somewhat arbitrarily) into a high temperature loss (above 350 °C) and low temperature loss (below 350 °C). Comparison of the Si/Al values from elemental analysis to those determined using NH_3-

TPD shows that ICP and TPD agree very well for the parent sample. This implies that virtually all Al atoms occupy tetrahedral framework positions and contribute to strong Brønsted acidity for these unmodified materials. However, such an agreement is very clearly not found for the desilicated material; the Si/Al ratio is significantly higher in the TPD measurements compared to elemental analysis. This is expected [1], and might indicate that a sizeable fraction of the Al does not contribute to any TPD-measurable acidity, in turn suggesting that extra framework Al is formed upon desilication. However, as the elemental analysis and the NH_3-TPD were performed for different desilicated samples, the discrepancy between elemental analysis and NH_3-TPD will not be further elaborated.

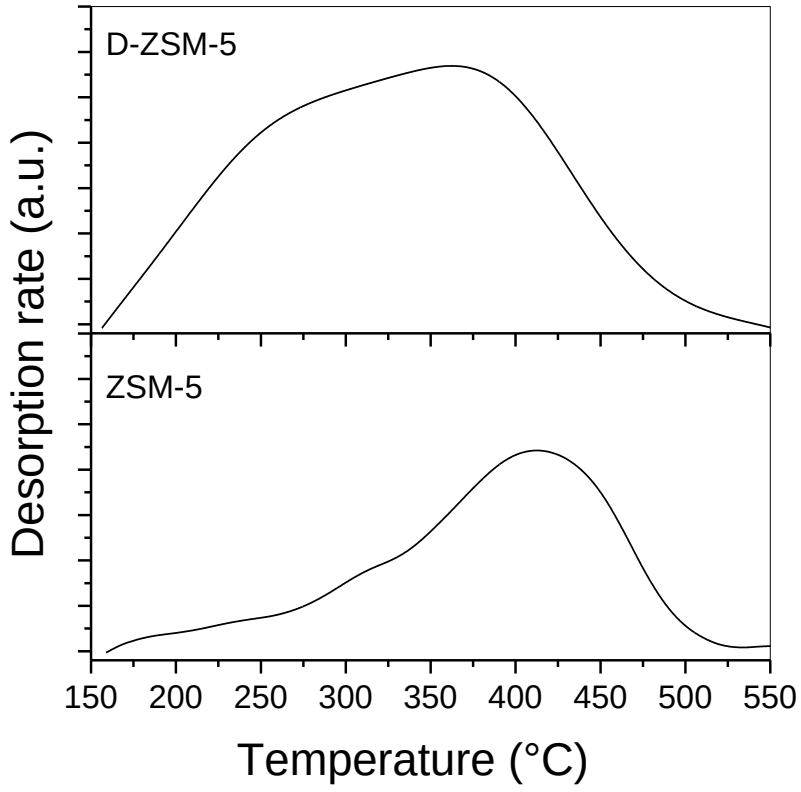

Figure S.4. Temperature programmed desorption of ammonia profiles for ZSM-5 (left panel) and D-ZSM-5 (right panel) as determined by means of thermogravimetry.

Table S.2. Aluminum content and distribution from elemental analysis and NH_3-TPD-TGA.

Catalyst	Si/Al ratio from ICP-MS	Si/Al ratio NH_3-TPD-TGA	NH_3 desorption below 350 °C (%)	NH_3 desorption above 350 °C (%)
ZSM-5	54	50	38	62
D-ZSM-5	19	26	50	50

The distribution and acidity of the hydroxyl groups on the fresh catalysts were evaluated by CO adsorption at liquid nitrogen temperature with IR spectroscopy. Figure S.5 compares the IR spectra of ZSM-5 and D-ZSM-5 samples activated at 450 °C. Spectra of the dehydrated catalyst and those obtained at the highest CO coverages are shown in black, while the intermediate coverages are represented with grey lines. For each experiment 60 mbar of CO was dosed on the activated sample which was subsequently cooled down to liquid nitrogen temperature. The spectra correspond to the progressive outgassing of the samples at low temperature. Two spectral ranges are of interest: 3800-2900 cm^{-1} (the region of ν(OH) bands) and 2300-2000 cm^{-1} (the region of ν(CO) band).

We will discuss the spectra of the dehydrated catalysts before CO adsorption first. Comparison of the two dehydrated samples (lower black curves) reveals that the component related to the external isolated silanols (peak at 3745 cm^{-1}) is much more intense and sharp for the desilicated sample than for the parent material. As reported previously [5], the desilication procedure leads to the formation of mesopores of fairly large diameter causing an increase in the number of apparently isolated species. The peak representing the strongly acidic Brønsted sites is seen at 3614 cm^{-1}, and the intensities of these absorptions are similar for the two catalysts, indicating a similar density of such sites. For the ZSM-5 catalyst, a very weak

component due to interacting silanols (so-called silanol nests, broad band centered at 3500 cm^{-1}) is seen, and these species are apparently removed upon desilication. Finally, a feature commonly attributed to partially extra-framework Al is observed at about 3663 cm^{-1}, and these species might be more abundant in the desilicated catalyst.

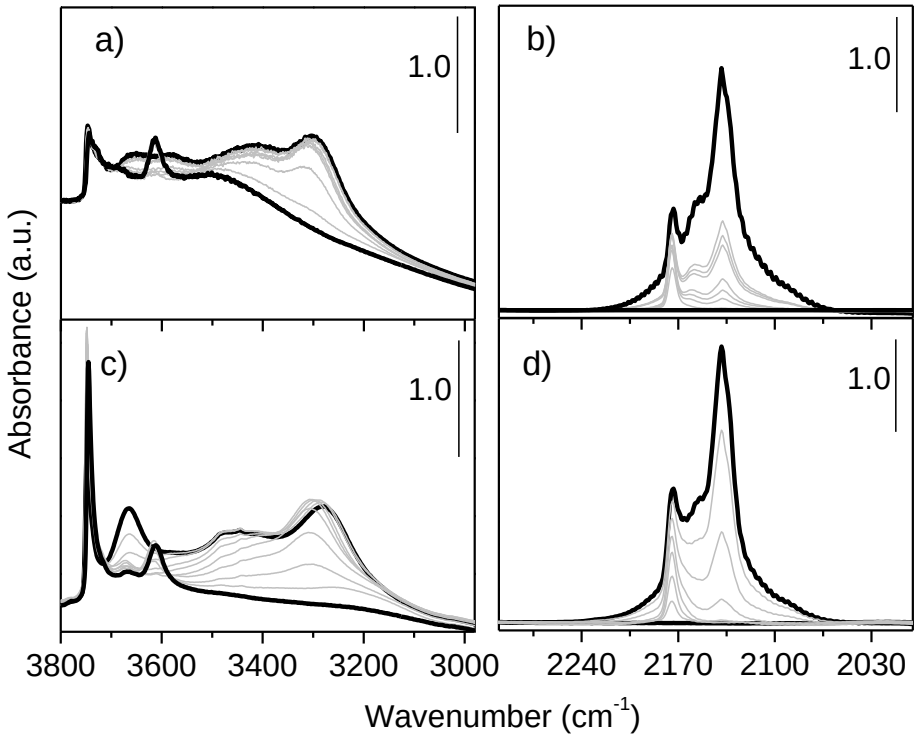

Figure S.5. FTIR spectra of CO adsorption at increasing coverages on ZSM-5 (upper part) and D-ZSM-5 (lower part) samples. Parts a) and c) report the spectra in the hydroxyl groups range (3800-3000 cm^{-1}) and parts b) and d) in the CO vibrational modes region (2300-2000 cm^{-1}), respectively. Black curves show the background spectrum and the highest CO coverage, while the grey curves report the intermediate adsorption steps.

Upon adsorption of CO, the ν(CO) stretching mode is shifted to higher frequencies compared to the gas phase: this shift is due to the interaction between CO and the zeolite acidic sites as a consequence of the formation of OH--CO adducts. The magnitude of this shift

is proportional to the interaction strength. Starting from low coverages, three components are visible at 2138, 2154, and 2172 cm^{-1}. Their assignments are: liquid-like CO, CO adsorbed on weakly acidic silanol sites or partially extra-lattice Al-OH (at 3663 cm^{-1}), and CO adsorbed on the strong acidic Brønsted sites [6,7,8,9]. Concurrently, the ν(OH) vibrations of the OH--CO adducts grow in a parallel manner at higher frequencies. As already described in the case of ν(CO), also here there is a direct proportionality between the strength of the interaction and the observed shift in vibrational frequency. The most acidic Brønsted sites (original band around 3614 cm^{-1}) give rise to a broad and intense band at 3300 cm^{-1} ($\Delta\nu$(OH) = -310 cm^{-1}), while the weaker sites (original band around 3663 cm^{-1}) are associated with a component centered at 3460 cm^{-1} ($\Delta\nu$(OH) = -200 cm^{-1}). Finally, the isolated silanol (original band at 3745 cm^{-1}) band gives rise to a component at 3665 cm^{-1} when perturbed by adsorbed CO ($\Delta\nu$(OH) = -80 cm^{-1}). Note that in this case, even at low temperature, not all of the silanols are completely eroded. The magnitude of these shifts agree well with those previously reported for both unmodified and desilicated H-ZSM-5 catalysts, and thus verifies that no unexpected surface hydroxyl species are abundant on the internal surfaces of the ZSM-5 and D-ZSM-5 catalysts. [1,10].

Figure S.6 shows the ring vibrational modes (1700–1400 cm^{-1}) of the irreversibly adsorbed portion of pyridine, i.e. the part that is not removed by evacuation at 150 °C. The band at 1554 cm^{-1} corresponds to pyridinum cations located on Brønsted acid sites, whereas the band at 1445-1442 cm^{-1} is assigned to pyridine coordinated to Lewis acid sites. The intense band at 1490 cm^{-1} results from both contributions [11]. As may be inferred from the spectra shown in Figure S.4, the concentration of Brønsted acid sites is mainly unaltered after desilication, only a moderate decrease in the intensity of the band at 1554 cm^{-1} is seen, in agreement with the direct observation of the the ν(OH) stretching modes of the Brønsted acid sites seen at 3614 cm^{-1} in Figure S.4 above. However, from the increase in the intensity of the

band at 1445-1442 cm^{-1}, it is evident that the concentration of Lewis acid sites increases considerably upon desilication. The ratio between Brønsted and Lewis acid sites increases from 6.0 for the parent ZSM-5 catalyst to 0.9 for the desilicated D-ZSM-5 catalyst. Finally, the data also show that there is an increase in the total amount of acid sites as a consequence of the alkaline treatment, which agrees well with the data from NH_3-TPD summarized in Table S.2.

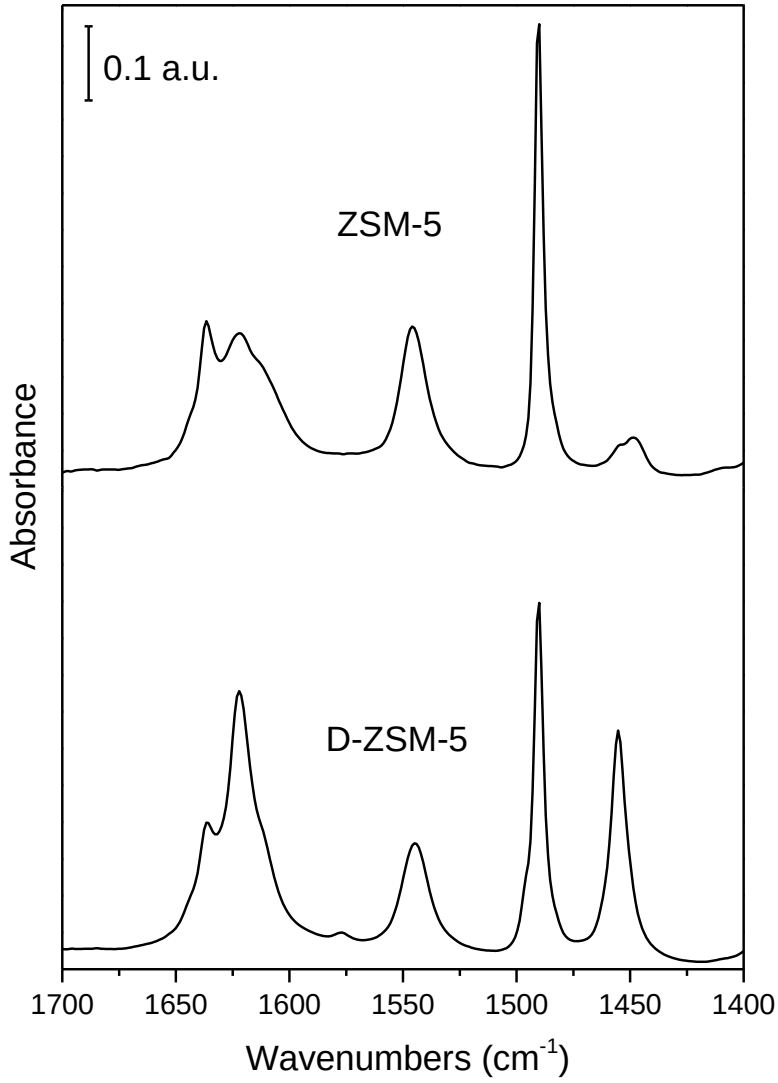

Figure S.6. FTIR spectra of pyridine adsorption after evacuation at 150 °C for the two catalysts.

2. Thermogravimetric analysis

Thermogravimetric analysis of partially deactivated catalysts samples was performed to determine the total content of coke.

Experimental

The total amount of oxidable hydrocarbons on the samples was determined by thermogravimetric analysis in a Rheometric Scientific STA 1500 instrument. About 15 mg of sample was used, and heated to 650 with a heating rate of 5 C/min. The final hold time at 650 °C was 2 h. The atmosphere was 4 mL/min O_2 + 8 mL/min N_2. The actual sample mass is plotted, and weight loss is given in percent of the mass of coke free sample.

Results

The TGA profiles for selected fractions of partially deactivated ZSM-5 are shown in Figures S.7-S.10 below.

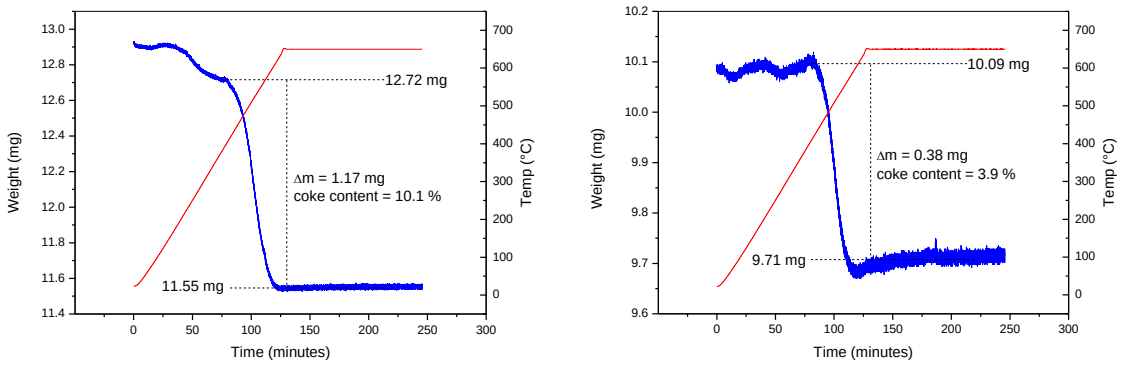

Figure S.7. TGA profiles for fraction 1 (left) and 2 (right) of partially deactivated ZSM-5.

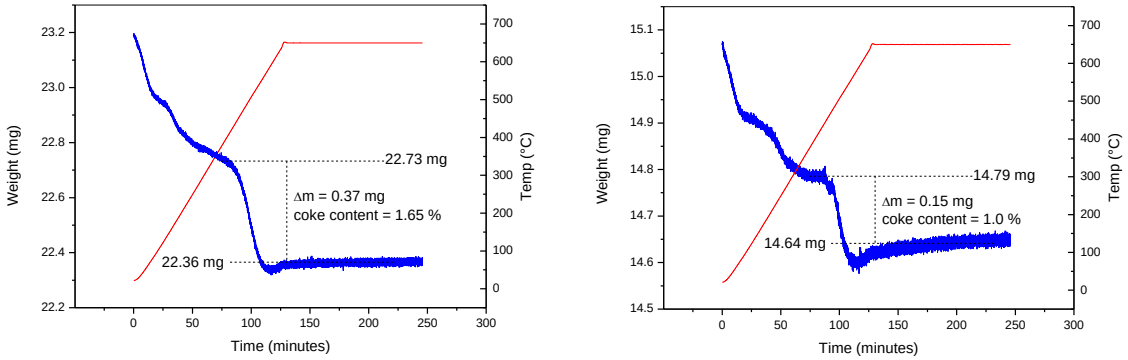

Figure S.8. TGA profiles for fraction 3 (left) and 5 (right) of partially deactivated ZSM-5.

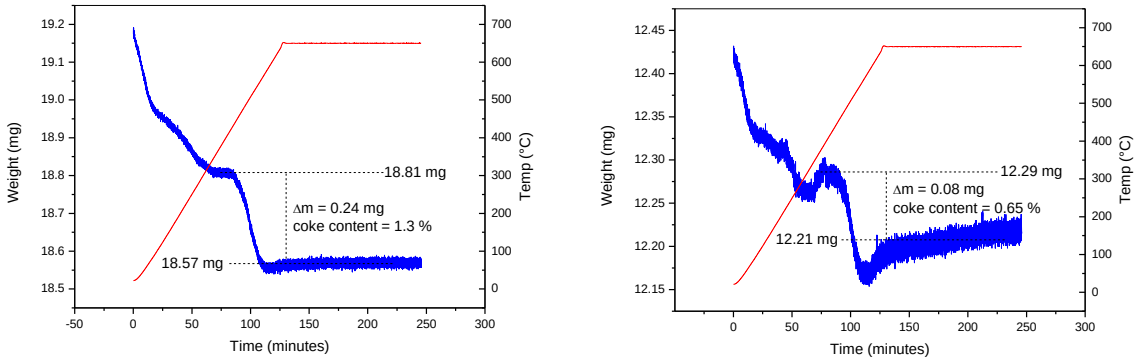

Figure S.9. TGA profiles for fraction 7 (left) and 9 (right) of partially deactivated ZSM-5.

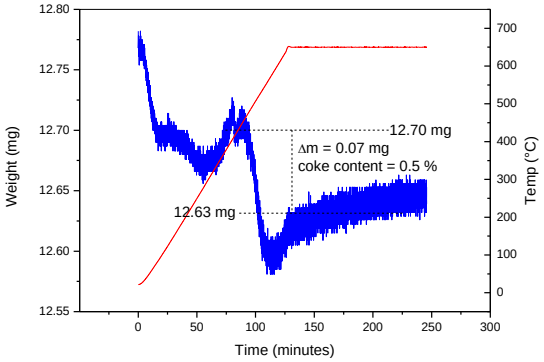

Figure S.10. TGA profile for fraction 10 of partially deactivated ZSM-5.

The TGA profiles for the fractions of partially deactivated D-ZSM-5 are shown in Figures S.11-S.13 below.

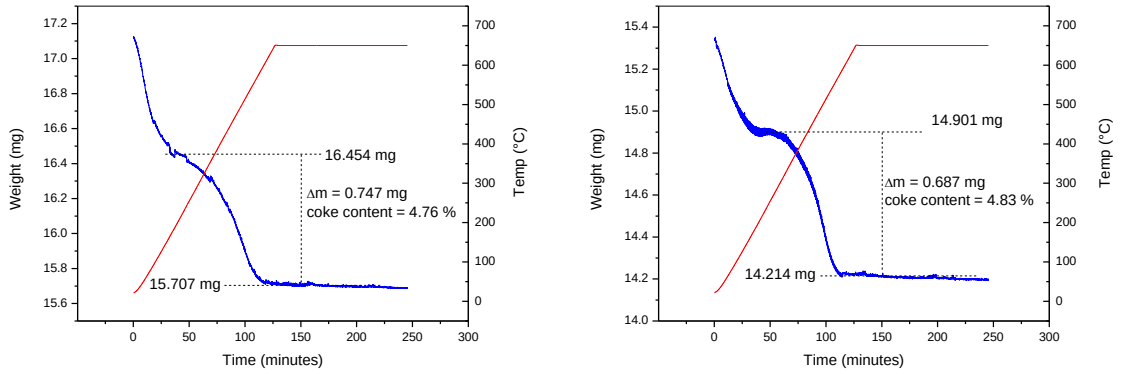

Figure S.11. TGA profiles for fraction 1 (left) and 2 (right) of partially deactivated D-ZSM-5.

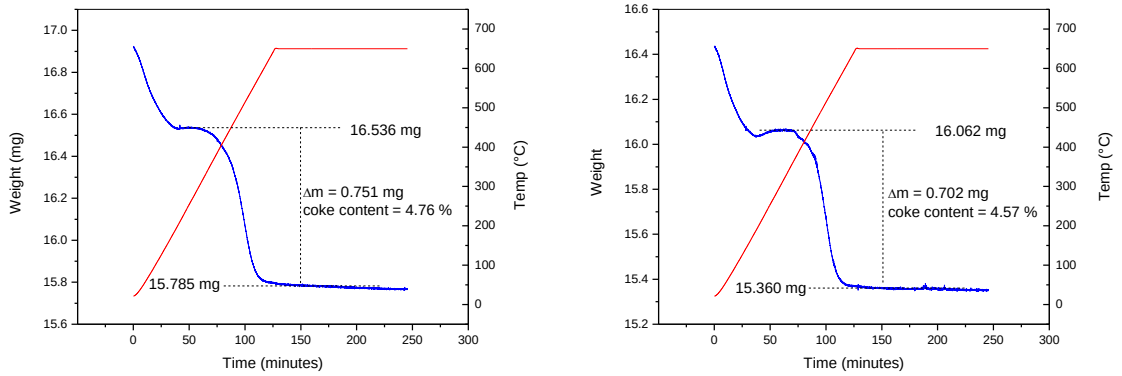

Figure S.12. TGA profiles for fraction 3 (left) and 4 (right) of partially deactivated D-ZSM-5.

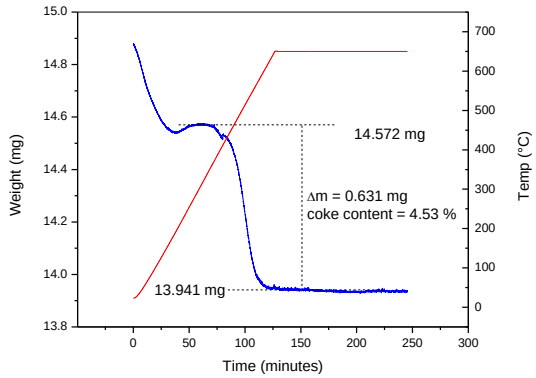

Figure S.13. TGA profile for fraction 5 of partially deactivated D-ZSM-5.

3. High mass resolution GC-MS

Experimental

High mass resolution GC-MS analyses were recorded applying a Fisons 8000 (Waters) Prospec-Q instrument, which is a hybrid mass spectrometer with EBEHQ configuration running at an acceleration voltage of 4 kV. Separation was carried out employing a DB-5MS column (30 m × 0.25 mm × 1 µm). The electron energy was set to 70 eV, and the source temperature was 250 °C. The mass resolution was 10000 (FWHM).

Results

The high mass resolution technique affords extremely accurate determination of the molecular mass of a given (molecular) ion, from which one can unequivocally determine the molecular formula. The peak at retention time = 20 min in the extracts of the D-ZSM-5 fractions was thus identified as $C_{11}H_{16}O$ (m/z = 164.119148), i.e. an oxygen containing compound. Based on the fragmentation pattern, the most plausible structure is given in Scheme S.1. The compound at RT = 27.6 min was identified as a hydrocarbon with molecular formula $C_{22}H_{30}$ (m/z = 294.232933). It seems reasonable to assume that this compound is formed by a condensation reaction between the $C_{11}H_{16}O$ species and methyl benzenes to give the compound shown in Scheme S.1.

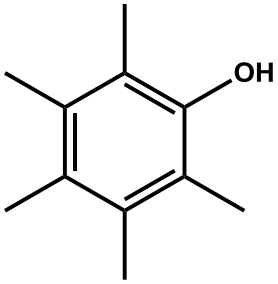

$C_{11}H_{16}O$

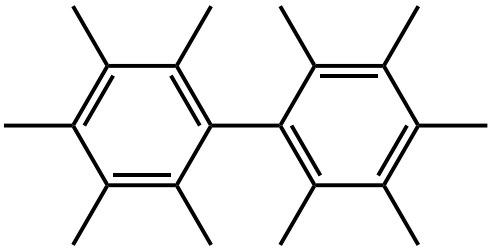

$C_{22}H_{30}$

Scheme S.1. Suggested molecular structures of compounds eluted at RT = 20 min and RT = 27.6 min in the coke extracts of the D-ZSM-5 fractions.

References

[1] S. Svelle, L. Sommer, K. Barbera, P. N. R. Vennestrøm, U. Olsbye, K. P. Lillerud, S. Bordiga, Y.-H. Pan, P. Beato, Catal. Today 168 (2011) 38.

[2] J. Perez-Ramirez, C.H. Christensen, K. Egeblad, C.H. Christensen, J.C. Groen, Chem. Soc. Rev. 37 (2008) 2530.

[3] K. Egeblad, C.H. Christensen, M. Kustova, C.H. Christensen, Chem. Mater. 20 (2008) 946.

[4] M. Ogura, E. Kikuchi, M. Matsukata, Stud. Surf. Sci. Catal. 135 (2001) 216.

[5] M. Bjørgen, F. Joensen, M. Spangsberg Holm, U. Olsbye, K.-P. Lillerud, S. Svelle, Appl. Catal. A 345 (2008) 43.

[6] C. Paze, S. Bordiga, C. Lamberti, M. Salvalaggio, A. Zecchina, J. Phys. Chem. B 101 (1997) 4740.

[7] S. Bordiga, P. Ugliengo, A. Damin, C. Lamberti, G. Spoto, A. Zecchina, G. Spano, R. Buzzoni, L. Dalloro, F. Rivetti, Top. Catal. 15 (2001) 43.

[8] A. Zecchina, S. Bordiga, G. Spoto, D. Scarano, G. Petrini, G. Leofanti, M. Padovan, C.O. Arean, J. Chem. Soc., Faraday Trans. 88 (1992) 2959.

[9] A. Zecchina, C.O. Arean, G.T. Palomino, F. Geobaldo, C. Lamberti, G. Spoto, S. Bordiga, Phys. Chem. Chem. Phys. 1 (1999) 1649.

[10] M. Spangsberg Holm, S. Svelle, F. Joensen, C. Hviid Christensen, S. Bordiga, M. Bjørgen, Appl. Catal. A 356 (2009) 23.

[11] J.A. Lercher, A. Jentys, Stud. Surf. Sci. Catal. 168 (2007) 435.